Iranian Journal of Chemical Engineering
Vol. 16, No. 2 (Spring 2019), IAChE

Research note

CFD Study of Mixing Concave Turbine in a Stirred Tank

A. Sinkakarimi, A. Ghadi [*]

Young Researchers and Elite Club, Ayatollah Amoli Branch, Islamic Azad University, Amol, Iran

ARTICLE INFO

Article history:
Received: 2018-07-28
Accepted: 2019-01-02

Keywords:
Concave Blade,
Rushton Turbine,
Power Consumption,
Mixing Time,
Optimum Impeller

ABSTRACT

Computational fluid dynamics (CFD) is a powerful numerical tool that is becoming widely used to simulate many processes in the industry. In this work, a study of the stirred tank with 7 types of concave blade with CFD was presented. In the modeling of the impeller rotation, sliding mesh (SM) technique was used, and RNG-k-ε model was selected for turbulence. Power consumption at various speeds in the single phase, mean tangential, radial and axial velocities in various points, effects of disc diameter and thickness, and mixing time were investigated. The optimum concave impeller was selected, and the effect of tracer feed position and probe location was investigated on it. Results suggested that power consumption was exactly dependent on impellers' scale and geometry; results are in good agreement with the experimental data, and turbulent flow is relatively independent of Reynolds number. Power number increases by increasing disc diameter for both concave and Rushton, and concave´s power is relatively independent of disc thickness; however, increasing it decreases Rushton´s power. The data revealed that the power number was 2.3±0.3 for a blade angle of 40°, whereas, for blade angles 25°, 50°, and 55°, it was 43 % lower and 57 % and 43 % higher, respectively.

1. Introduction

Mixing is one of the most common operations in chemical processes, and the knowledge of fluid flow pattern can considerably help optimize the operation. A large number of process applications involve a mixture of single-phase flows in mechanically stirred vessels. The optimum design and the efficiency of mixing operations are important parameters in product quality and production costs; hence, awareness of different characteristics such as velocity distribution profiles and turbulence parameters in the optimization of the vessels is critical. The flow motion in stirred tanks is 3-dimensional and the flow is highly turbulent around the impeller. For a long time, the design of mixing systems was determined experimentally. This approach was time-consuming and expensive and process scale-up was based on empirical rules established on pilot rigs. In recent years, computational fluid dynamic techniques have been increasingly used as a substitute for an

[*]Corresponding author: arezoo.ghadi@gmail.com

experiment to obtain the details of the flow field for a given set of fluids, impellers, and tank geometries [1,2]. Rushton turbine is a traditional six-blade disc turbine, which is widely used. The flat blade of the Rushton turbine leads to the formation of a pair of high-speed, low-pressure trailing vortices at the rear of each blade [3,4]. Recently, different modifications in the blade geometry have been considered such as shaping the blade from a flat plate to one with various degrees of streamlining in cross-section. These new curved blade turbines have a cavity structure. The original concave blade concept was developed in the 1970s at Delft University by a group led by Jhon M.Smith. Van´t Riet et al. (1976) studied a variety of impeller styles and introduced the concept of concave blades [5]. Wong, C.W. et al. (1988) studied the curved-blade turbine [6]. Warmoeskerken and Smith. (1989) extended that work and explained the improved performance of the concave blades compared to flat blades [7]. The newer blade designs with deeper concavity were proposed by Hjorth (1988) and Middleton (1993) [8,9]. Galindo, E. et al. (1993) studied a similar design on parabolic-blade Scaba 6SRGT [10]. Bakker et al. (1994) studied the performance of impellers with a semicircular blade shape, the Chemineer CD-6 [11]. A comparative analysis of the fluid dynamic performance of the concave turbines and hydrofoil impellers was provided by Neinow.A.W (1996) [12]. Bakker et al. (1998) designed a new impeller BT-6 that has been optimized to take into account different flow conditions above and below the disc [13]. D.Pinelli et al. (2003) studied the behavior of the asymmetric concave blade (BT-6) and compared it with the behavior of other impellers [14]. S.D.Vlaev et al. (2004) reported the distribution of pressure in some radial flow impellers such as parabolic and circular concave blade impellers and a conventional flat-blade Rushton turbine and, then, compared impellers [15]. Liu Xinhong et al. (2010) investigated the turbulence structure in the stirred tank with a deep hollow blade (semi-ellispe) disc turbine (HEDT) by using time-resolved particle image velocimetry (TRPIV) and traditional PIV [16]. Jing ZHAO et al. (2011) analyzed trailing vortices and elucidated their relationship with turbulence properties by four different disc turbines: Rushton, concaved, half elliptical, and parabolic blades. Results showed that the blade shape had a great effect on the trailing vortex characteristics [17]. Afshar et al. (2013) analyzed the determining factors in power of curved blade impellers in both aerated and un-aerated conditions. The results indicated that the curvature angle and central disk size were significant parameters through variance analysis, and significance of the central disk size was less than that of the other variables [18]. In 2016, Houari Ameur studied the effect of the impeller blade curvature on mixing characteristics. He determined the blade design in retreat shape, which seems very promising in terms of power consumption since a reduction in Np is obtained by increasing blade curvature [19].

2. Methodology

The CFD modeling involves the numerical solution of the conservation equations in the laminar and turbulent fluid flow regimes. Therefore, the theoretical predictions were obtained by simultaneous solution of the continuity and the Reynolds-Averaged Navier-Stokes (RANS) equations. The continuity and momentum equations for incompressible and Newtonian fluids are as

follows:

$$\frac{\partial u_j}{\partial x_i} = 0 \quad (1)$$

$$\frac{\partial u_i}{\partial t} + u_i \frac{\partial u_j}{\partial x_i} = -\frac{1}{\rho}\frac{\partial p}{\partial x_i} + \nu \frac{\partial^2 u_i}{\partial x_j^2} - \frac{\partial \tau_{ij}}{\partial x_j} \quad (2)$$

$$\tau_{ij} = \left(\frac{\partial u_i}{\partial x_j} + \frac{\partial u_j}{\partial x_i}\right) \quad (3)$$

where u_i is the velocity in the i^{th} direction, ρ is the density, p is the pressure, ν is the kinematic viscosity of the fluid, and τ_{ij} is stress tensor. For turbulent flow, the above set of equations will have to be solved with Direct Numerical Simulation (DNS) to obtain the true variation of the velocity field. The governing equations are time-averaged Navier-Stokes equations, and the results are discretized and linearized by the finite volume method.

2.1. CFD method

A three-dimensional CFD simulation was carried out in order to model the behavior of cylindrical stirred vessels with a concave impeller and a Rushton turbine for complex configurations. A computational grid consisting of two parts: an inner rotating cylindrical volume enclosing the turbine; an outer, stationary volume containing the rest of the tank. The structured grids composed of non-uniformly distributed hexahedral cells were used in the two parts. The grid used in the impeller region was densified to get a more accurate description of the impeller. The total number of grid nodes was 400000 in the tank. In this study, the MRF solution was used as a starting point. The simulation was then switched to unsteady SM model and first-order upwind scheme for discretization; in addition, the SIMPLE algorithm for pressure velocity coupling was used. Water at 25 °C was used as the test fluid ($\mu=10^{-3}$ Pa.s, $\rho=998.2$ kgm^{-3}). Dimensions of the stirred tank and details of concave and Rushton impellers are shown in Fig. 1 and Tables 1 and 2. In all impellers, E=E´ and A-A slice is the disk placement.

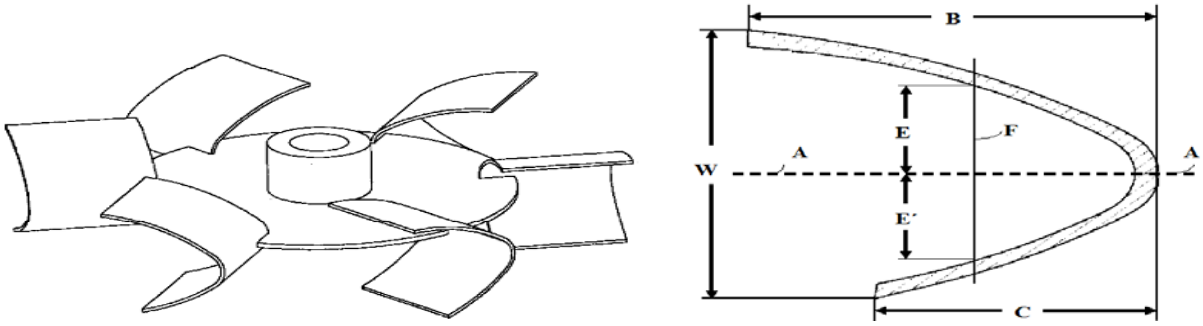

Figure 1. The Concave impeller with vertically asymmetric blades.

Table 1
Dimensions of the stirred tank and Rushton impellers.

Value(m)	Tank diameter	Impeller diameter	Disk diameter	Disk thickness	Blade height	Blade length	Blade thickness	Blade angle	Baffle length	Bottom clearance
Rushton Standard	0.3	0.1	0.066	0.0017	0.02	0.025	0.001	45	0.03	0.01
Rushton with same surface of Concave4	0.3	0.1	0.066	0.0017	0.02	0.0415	0.001	45	0.03	0.01

Table 2
Dimensions of the stirred tank and Concave-blades impellers.

Impeller	Concave1	Concave2	Concave3	Concave4	Concave5	Concave6	Concave7
Tank diameter(m)	0.3	0.3	0.3	0.3	0.3	0.3	0.3
Impeller diameter(m)	0.1	0.1	0.1	0.1	0.1	0.1	0.1
Disk diameter(m)	0.066	0.066	0.066	0.066	0.066	0.066	0.066
Disk thickness (m)	0.035	0.035	0.035	0.035	0.035	0.035	0.035
Blade height(m)	0.025	0.025	0.025	0.0125	0.0375	0.025	0.050
Blade length(m)	0.025	0.025	0.025	0.025	0.025	0.025	0.025
Blade thickness(m)	0.002	0.002	0.002	0.002	0.002	0.002	0.002
Blade depression (B-C)	0.00375	0.00625	0.0125	0.00625	0.00625	0	0
Blade angle(degree)	40	40	40	25	50	40	55
Baffle length(m)	0.03	0.03	0.03	0.03	0.03	0.03	0.03
Bottom clearance(m)	0.01	0.01	0.01	0.01	0.01	0.01	0.01

2.2. Investigation of mesh density effect

Before conducting the simulation, it is necessary to ensure the correctness of the mesh and its density. In other words, the effect of the size of the control volumes on simulation results based on the prediction of fluid hydrodynamic characteristics should be investigated. Therefore, it is always essential to get the best and most accurate answers with the lowest number of mesh, which depends on the desirable accuracy of the problem. Therefore, determining the optimal mesh density in each simulation operation is necessary. For this purpose, several models with different mesh densities have been studied, which vary at the time of computer computing and reaching the constant energy distribution in the total volume of the tank. First, it appears that increasing the density of the no-blade region without increasing the number of cells in the rest of the tank volume can increase the accuracy of the results, while the calculation time is reduced. Several structures of this type have been studied, and it is observed that when the difference of density between the two regions increases, the computational stability decreases sharply. Therefore, it is practically impossible to select the density with high difference uniformity between the two regions. In this work, with several guessing and error, the difference in mesh density between two and outer regions is selected. By increasing mesh density and repetition of calculations, the results for radial velocity distribution are shown in Fig. 2. The radial velocities (V_r) are normalized by tip velocity, which are defined as the maximum velocity of the fluid jet, and are plotted in z/H, where z is the vertical distance from the tank floor, and H is the tank height.

$$V_{tip} = \pi ND$$

where D is the diameter of the blade, and N is the blade rotational speed.

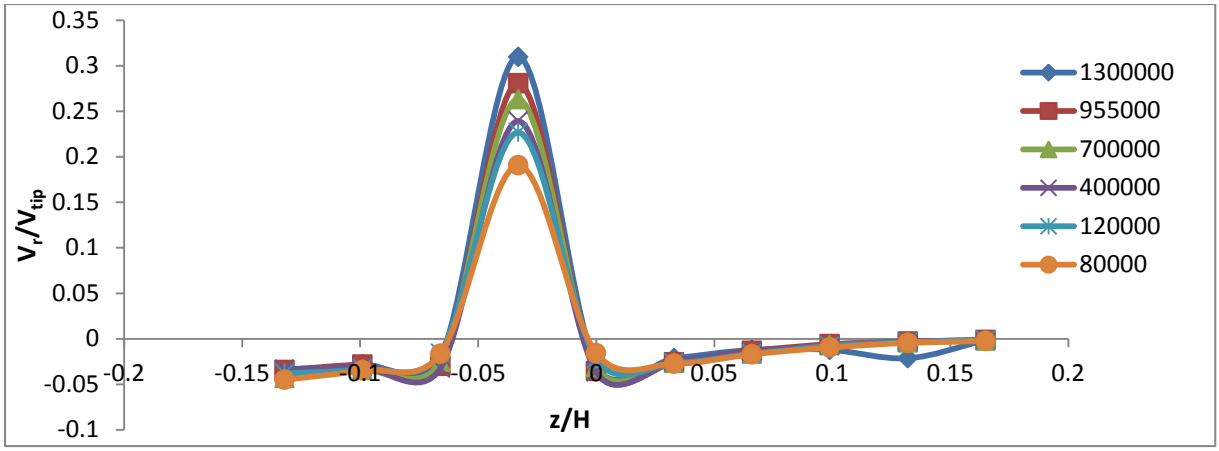

Figure 2. Comparison of radial velocity values obtained from simulation of concave2 with mesh densities of 80000, 120000, 400000, 700000, 955000, and 1300000 at r/R = 0.37.

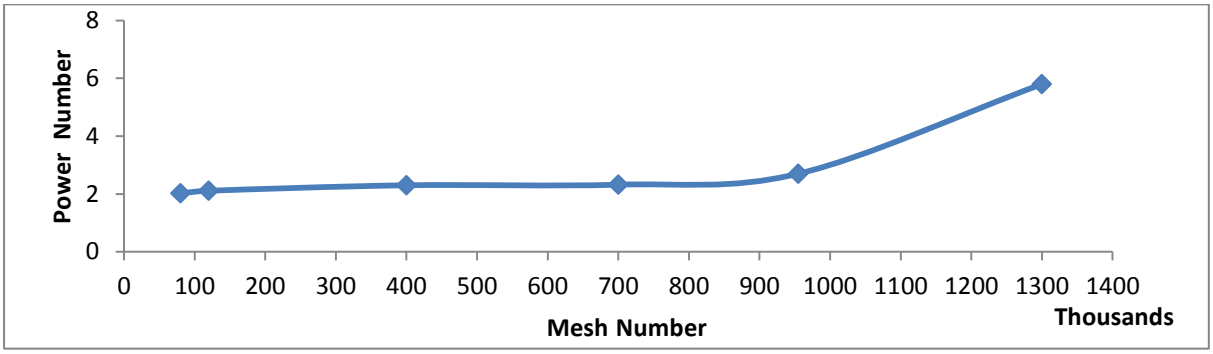

Figure 3. Effect of mesh number on power number of concave2.

To evaluate Rushton density, results of the radial velocity distribution in comparison with the results of Wu and Patterson experimental [20] are shown in Fig 4. The radial velocities are normalized by tip velocity and are plotted in 2Z/W, where Z is the axial distance of the blade disc, and W is the Rushton's blade height.

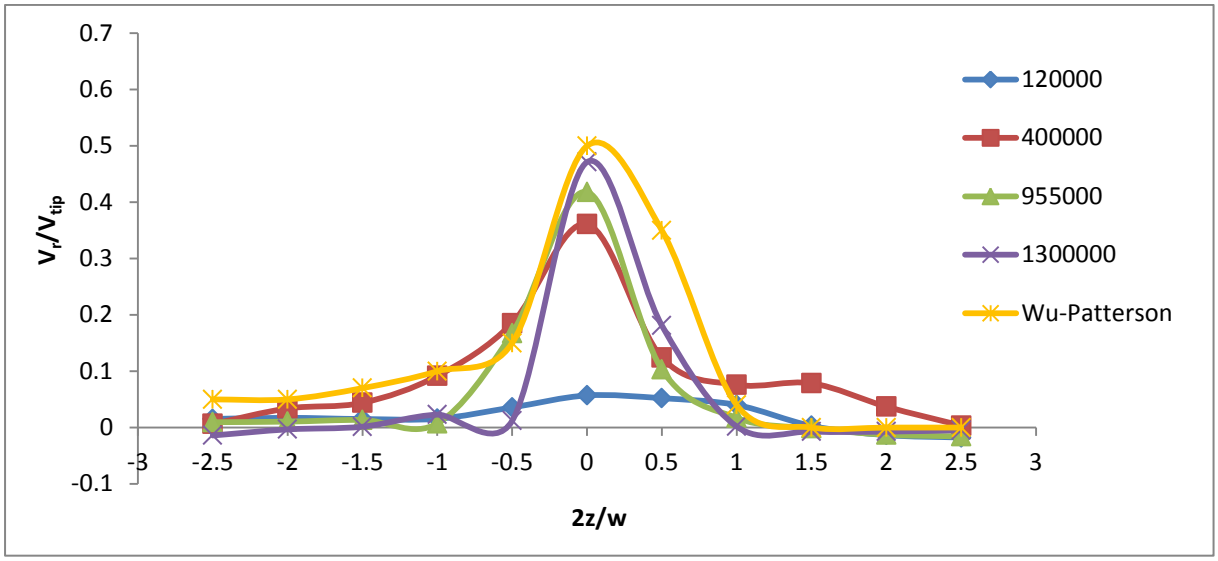

Figure 4. Comparison of radial velocity obtained through Rushton simulation at 12000, 400000, 955000, and 1300000 mesh densities and experimental results at r/R =0. 37.

As shown in Figs. 2 and 3, by increasing the number of meshes, the maximum radial velocity increases, and the accuracy of the results of the simulation also increases. Further, Fig. 3 shows that, in 400,000 meshes, the simulation results are fixed and the number of meshes does not affect the results; however, in very high density, it suddenly increases. The results of the Rushton mesh density in Fig. 4 show that with increasing the number of meshes, the results of radial distribution of velocity vectors are highly consistent with experimental data. Therefore, in high densities, despite the improvement of the accuracy of calculations, due to acceptable accuracy at lower densities in all tank areas and due to a significant reduction in computation time, lower densities are acceptable. Eventually, CFD simulation has been done on 400,000 meshes.

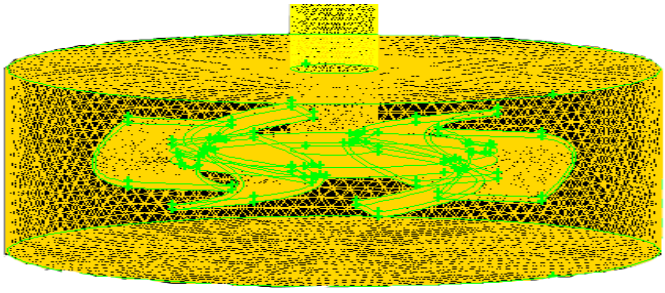

Figure 5. Inner volume of a concave impeller with hexahedral mesh for clockwise rotating.

2.3. Power consumption

An accurate CFD model should be able to predict important parameters such as the overall power input to a stirred tank. The flow field around the impeller and, also, the shear stress and the pressure distribution on the impeller blade are resolved. Then, power can be directly estimated by a calculation of the total torque required to rotate the impeller. The torque on each blade can be calculated as follows [21, 22, 23]:

$$\Gamma = \sum (\Delta p_i) A_i \, r_i \qquad (4)$$

where the summation is over the control cells i corresponding to each blade, Δp is the pressure difference between the front and the back sides of the blade at the surface element i, A_i is the effective surface of each blade, and r_i is the radial distance from the axis of the shaft on which the impeller is mounted. The power required to rotate the impeller with m blades at a steady rotational speed of N revolution per second is given by:

$$P = 2\pi N m \Gamma \qquad (5)$$

The power consumption, P_p, is described by a power number, N_p, which depends on fluid properties and on the geometrical parameters of a mixing device that can be computed as follows:

$$N_p = \frac{p}{\rho N^3 D^5} \qquad (6)$$

where ρ is the density of a tank fluid, and D is the impeller diameter [24].

2.4. Estimation of mixing time

Mixing time is the time taken from that moment when a specific volume of fluid is added to the fluid in the mixing vessel and blended in it with a pre-chosen degree of uniformity [25]. The progress of mixing is specific to the flow field, which is characterized by a circulation pattern and effective diffusivity. For turbulent flows, the

molecular diffusivity is augmented by turbulent fluctuations, and the effective diffusivity, being a strong function of local velocity gradients, becomes a flow property. In a real stirred tank, there are large vortices and final macro-instabilities, which promote tracer mass exchange through this boundary. The progress of mixing in a given flow situation can be visualized by introducing a virtual tracer and monitoring how its concentration (or it´s a mass fraction) changes with time.

3. Results and discussion

3.1. Flow field

The velocity vector plot of the mean flow field is located on the perpendicular plane crossing impeller center, are shown in Fig. 6. Fig. 6 shows the orientation of the impeller discharge stream and ring vortices formed around the impeller disc. The flow splits on the wall and two separate circulation flow patterns emerge: one on the upper side of the surface of the vessel and another along the wall to lower circulation zone and, then, both of them axially along the shaft returning to the center of the impeller and pumping to walls by jet flow of impeller. As is shown, the circulation pattern in Rushton, especially in lower circulation zone, is stronger than concave.

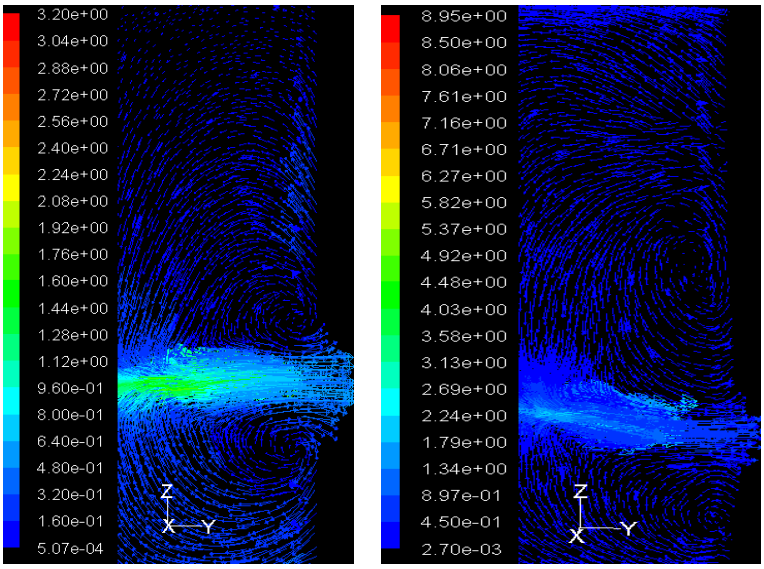

(a) (b)

Figure 6. Velocity field (m/s) along a cross-section of the tank in the middle of the tank for N=400(rpm). (a) Concave impeller, (b) Rushton impeller.

Figs. 7, 8, and 9 show axial, radial, and tangential velocities, respectively, along the tank height and r=12cm for seven concaves and Rushton at the impeller rotational speed of 400 rpm. The velocity data are normalized by tip velocity, V_{tip}=ΠND.

Axial profile shows the upper part of the tank fluid moving upward along the wall and, then, flowing downwards to form a loop on the vertical plane. Another circulation loop exists in the lower part of the tank. The maximum axial velocity appears in the region where the fluid is sucked into the impeller blades. At r =12 cm (r/R=0.8), normalized mean axial velocity almost vanishes. This is about the place where the stream is split into two streams: one flowing upward and the other flowing downward. Further, it is observed that the axial velocity distribution of concaves and Rushton is very near to each

other. Radial mean velocity shows that the impeller stream flows away from the impeller blades and the velocity varies dramatically in the axial direction. As the fluid moves away from the impeller, the velocity profiles in the impeller stream become flattered. The maximum radial velocity occurs near the tip blade. As observed in areas near the impeller, Rushton outperforms most of the concaves, but by increasing radial distance, it has a weaker operation than concaves. Tangential flow is in the vectorial direction of impeller rotation.

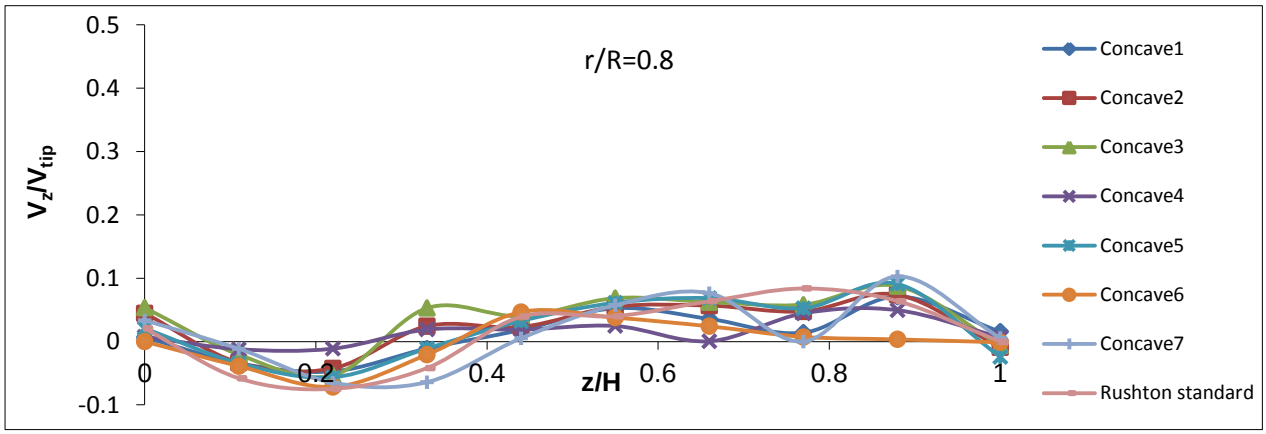

Figure 7. Normalized mean axial velocity profiles at 12 cm in N=400rpm

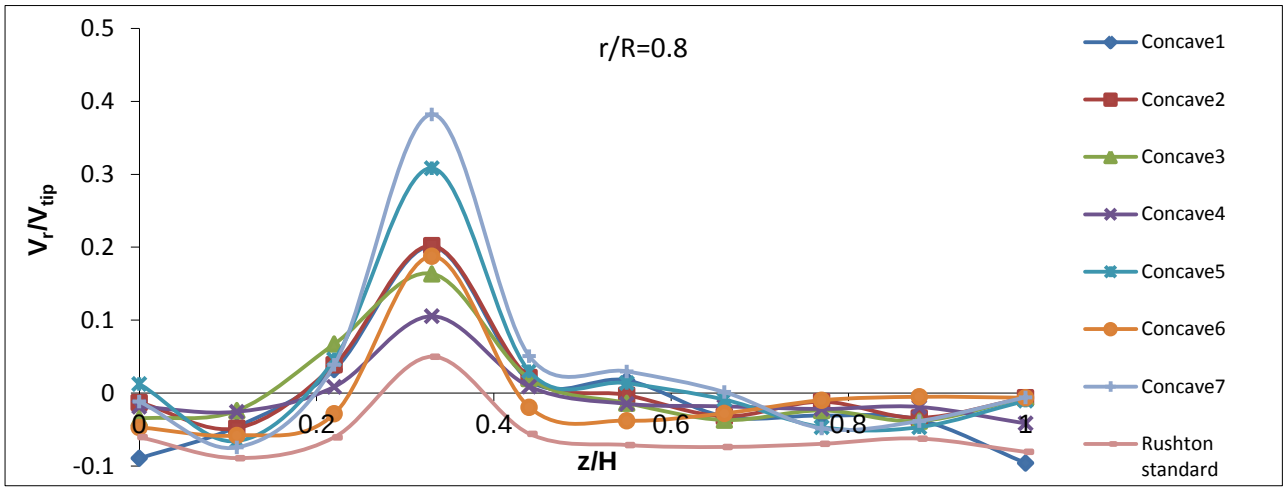

Figure 8. Normalized mean radial velocity profiles at 12 cm in N=400rpm.

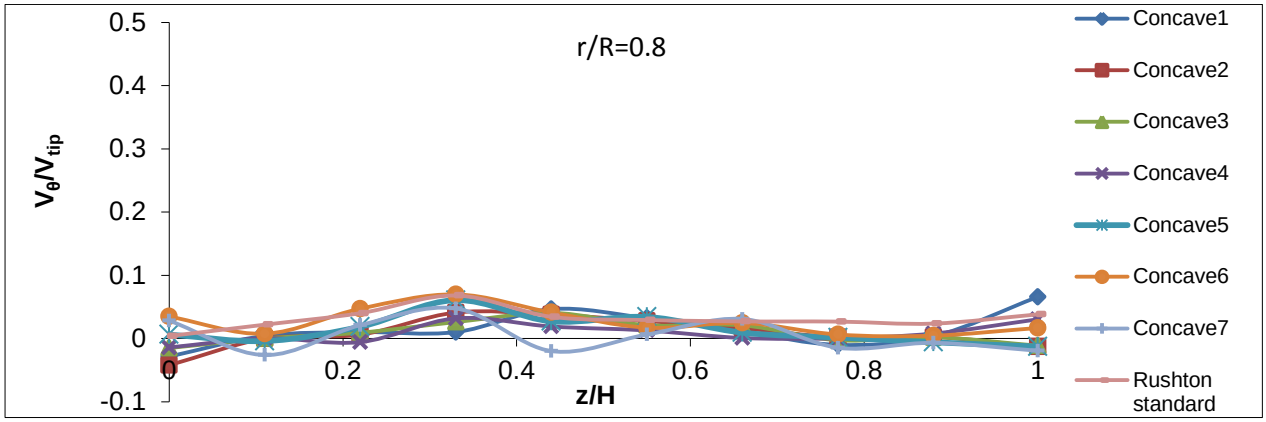

Figure 9. Normalized mean tangential velocity profiles at 12 cm in N=400rpm.

As is shown in Fig. 6, maximum tangential velocity increases with increasing blade angle. It appears that as the curvature of concave blade increases, the axial, radial, and tangential jets become weaker.

3.2. Power number

The impeller power number (N_p) is commonly used to check the validity of CFD simulations of the flow in stirred tanks [24, 26]. In this work, the pressure distribution on the impeller blade is resolved. Fig. 10 shows the pressure distribution on a horizontal plane through the impeller. For Rushton, a low-pressure region is in the front, and high-pressure region is in the back of each blade and, for concave, is in reverse. As is shown, for concave impeller, the high-pressure section of each blade affects the low-pressure section of the next blade.

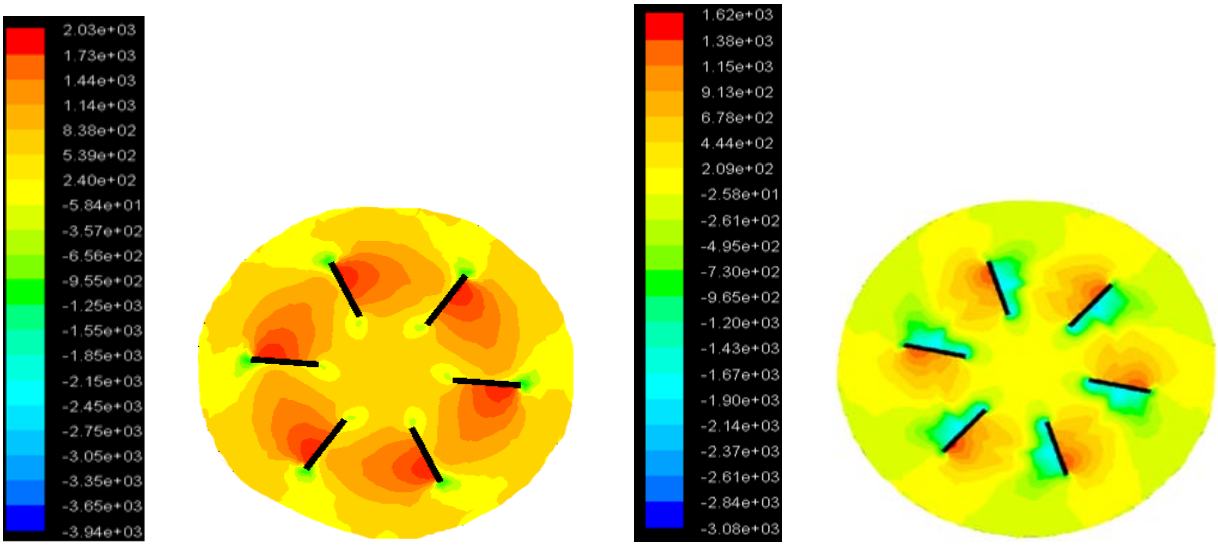

Figure 10. Pressure distribution in a horizontal plane through the impeller.

By using Eqs. (4) to (6), power numbers in velocities (N=50 to N=550 rpm) were calculated and compared to each other. Fig. 11 indicates the results of power consumption under turbulent flow conditions. As is shown, power is dependent on the shape and exact geometry of the impeller. The turbulent power numbers of Concaves 1, 2, and 3 are 2.3±0.3 that are approximately equal to BT-6 power number [27]. The Concave4 power number for the turbulent mixing regime is as low as 1.0±0.1 and for Concaves 5 and 7 are 4.0±0.1 and 5.3±0.3, respectively. The power numbers of Concave6 are 2.0±0.1 that correspond to the parabolic hollow-blade impeller power number predicted by CFD approximation of the experimental values 1.7±0.3 [15]. Results are also compared with Rushton standard and Rushton with the equal surface of Concave4, showing that, on the same surface, the concave impeller has lower power than Rushton.

3.2.1. The effect of the turbulence model on power consumption

Power levels of impellers were calculated by various turbulent models and were compared with each other. It is observed that the power of each impeller in the same velocities is relatively independent of the turbulence model, and this case is more visible with increasing Reynolds number. The results are shown in Fig. 12.

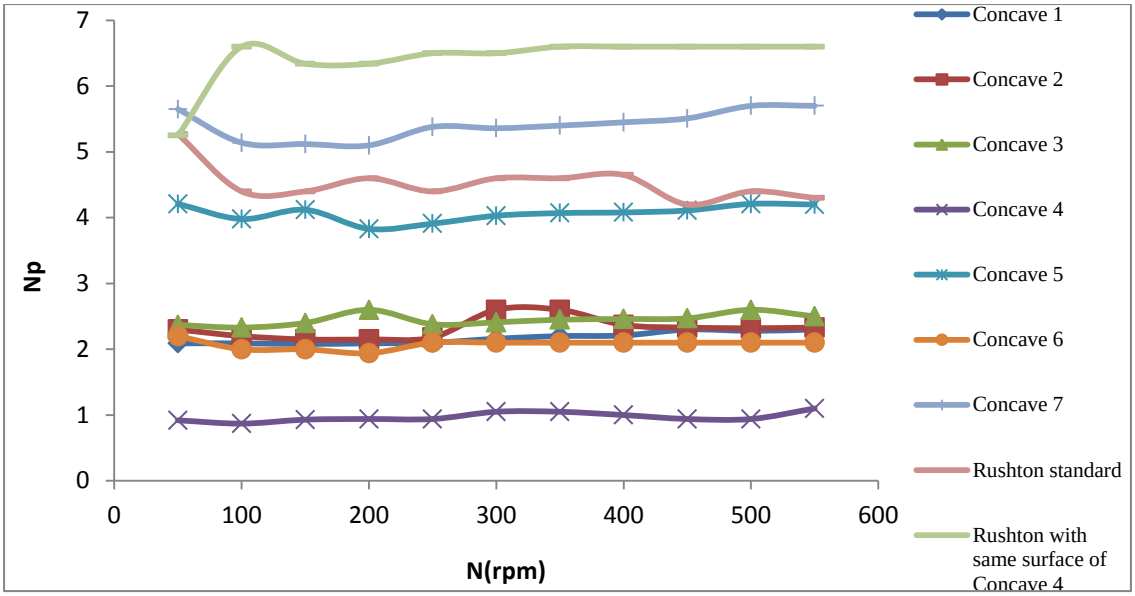

Figure 11. Investigation of power consumption with increasing the impellers' rotational speeds.

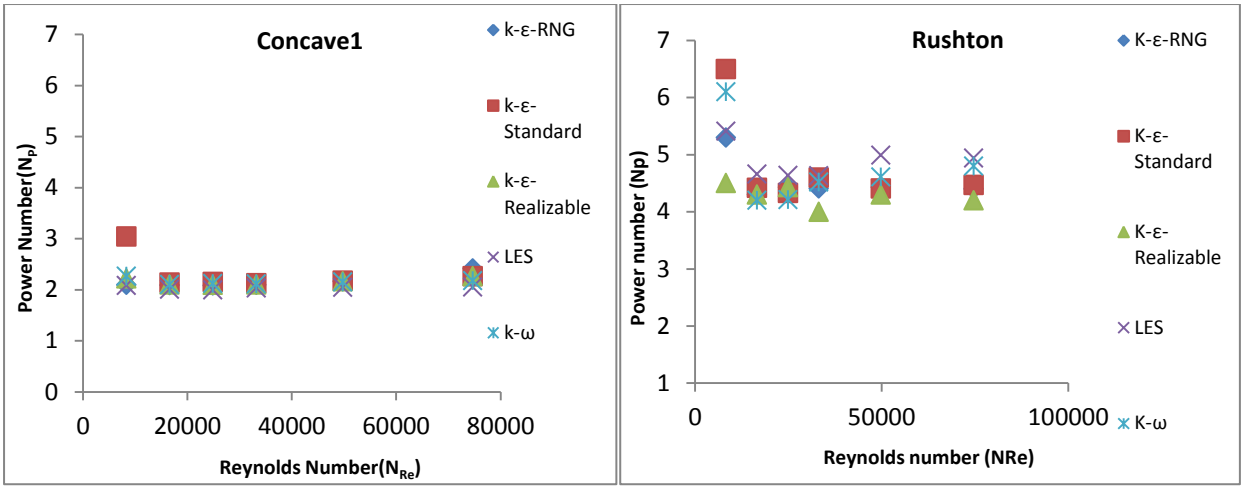

Figure 12. Investigation of power number in various turbulence models.

3.2.2. The effect of impeller design parameters on power consumption

Parameters given in Tables 3 and 4 were used to investigate power consumption. The tank diameter, baffle length, and other dimensions are kept constant in all simulations.

Table 3
Different values for disc thickness.

D/T	x/D	D_0
1/3	0.017	2/3 D
1/3	0.025	2/3 D
1/3	0.035	2/3 D
1/3	0.04	2/3 D

Table 4
Different values for disc diameter.

D/T	x/D	D_0
1/3	0.035	0.66 D
1/3	0.035	0.7 D
1/3	0.035	0.75 D

Figs. 13 and 14 depict that a decrease in disc thickness causes an increase in Rushton power, and it does not relatively affect the concave power number; an increase in the disc diameter causes an increase in the power of both Rushton and concave impellers. Decreasing Rushton´s N_p with increasing disc

thickness can be explained: as x increases or gets closer to the blade height, w, the momentum exchange between the liquid and the impeller in the θ direction gets more and more restricted, which in turn results in a decrease in the power delivered to the liquid by the impeller [28].

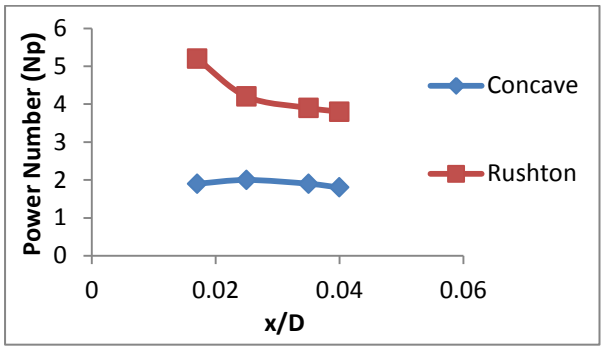

Figure13. Effect of the disc thickness on the power number.

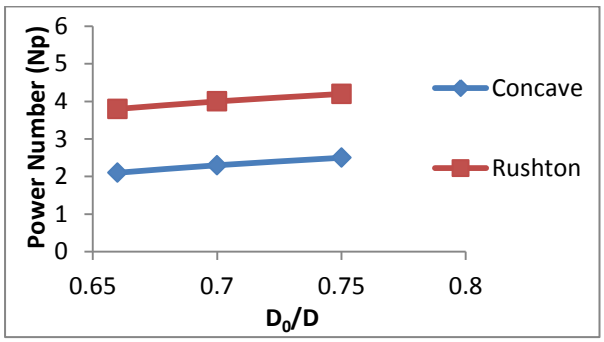

Figure14. Effect of the disc diameter on the power number.

3.3. Mixing time

A pulse injection of sodium-sulfate as a tracer in t_{inj} = 1/2 s is done just below the free liquid surface at the opposite direction of the concentration sampling point. Injection point was located just above the interface because the inner mesh volume is the main promoter of the distribution of the tracer and, close to the sliding mesh boundary, there is no tangential exchange of the tracer between the velocity flow loops in the baffles [29]. Mass fraction of the tracer was recorded at the sampling point, which was placed between two baffles, 8 cm below the liquid surface and 5 cm from the tank wall. Each normalized signal starts from concentration C(t=0)=0 and changes over time into the concentration of C(t=∞). The mixing time (t_{95}) is defined as the time needed to get 95 % homogeneity or to reach 95 % of the final concentration in the tank. Table 5 shows the results of mixing time for concave and Rushton impellers in N=400 rpm. As is shown, Concave4 with a minimum angle has maximum mixing time, Concave6 with a maximum angle and blade height has minimum mixing time, and Concave5 with a major angle and blade height of other impellers has a lower mixing time. In the state of the equal angle, for Concaves 1, 2, and 3, mixing time changes with variations in the low-depression section of blades. Therefore, Concave3 with the highest depression has lower mixing time; then, Concave2 and Concave1 with respective depressions in the measure of 1/2 and 1/4 of Concave3 have major mixing times. Further, mixing time was calculated for two Rushtons: first, ($Rushton_1$) the disc thickness is equal to the concaves (0.035D); another one, ($Rushton_2$) the disc thickness is equal to (0.017D).

Table 5
Results of mixing time for Concave and Rushton impellers in N=400 rpm.

Impeller	Mixing time($t_{95\ \%}$, s)	Mixing time($t_{99\ \%}$, s)
Concave1	10.7	16.47
Concave2	10.61	16.33
Concave3	9.32	14.35
Concave4	16.53	25.45
Concave5	8.06	12.41
Concave6	11.76	18.11
Concave7	5.78	8/9
$Rushton_1$	12.38	19.06
$Rushton_2$	9.62	14.81

3.4. Optimum impeller

Power consumption and mixing time of a

mixing system are key variables in chemical and bioprocess engineering; therefore, these variables should be examined to select the optimum blade. According to the investigation into concave and Rushton impellers, it was shown that power consumption increased with blade angle and had a reverse relation with mixing time; however, since mixing time is a more important variable than power consumption in a mixing system, it is given top priority to select the optimum impeller. Concave1 with high mixing time and Concaves 5 and 7 with high power could not be optimized; therefore, other 4 Concaves with the same blade angle is compared with Rushton. Between of these impellers, Concave3 has the lowest mixing time, and power consumption rates of these 4 Concaves are almost similar to each other and are different by 2.3 ± 0.3 that are lower than Rushton. Power of Concave3 is slightly higher than that of the other 3 concaves; however, because of lower mixing time, this impeller is selected as the optimum impeller, compared to other concaves and Rushton turbines.

3.4.1. The effect of probe location on mixing time of the optimum impeller

The location of the probe changed in five points above and below the impeller, and the same scale of tracer was injected at the injection points. All probes were placed between the baffles and located at a distance of 5 cm from the tank wall. The probes above the impeller (P_1, P_2, P_3) were placed at off-bottom clearance of 22, 18, and 14 cm, respectively, and probes below the impellers (P_4) and (P_5) were placed at off-bottem clearance of 7 and 4 cm, respectively. Table 6 gives the mixing times for these five probes with the injection above the interface. Results show that mixing time for probes under the impeller is lower than that above it. It is implied here that, under the blades, axial exchange current is stronger than the upper side of the blades, which causes faster uniformity of the tracer in the tank. Moreover, for probes above the impeller, mixing time decreases as the detection height moves toward the injection point and decreases as the detection height moves toward the impeller for probes at the bottom of the impeller.

Table 6
Mixing time of the optimum impeller for different probes.

Probe number	Mixing time($t_{95\ \%}$, s)	Mixing time($t_{99\ \%}$, s)
P_1	9.32	14.35
P_2	9.66	14.87
P_3	9.76	15.03
P_4	6.39	9.84
P_5	6.6	10.16

3.4.2. The effect of the injection position on mixing time of the optimum impeller

The point of injection varied in six points on the top and the wall of the optimum impeller vessel. The schematic diagram of the vessel showing the positions of the tracer injection points is shown in Fig. 15. The example of fluctuations in concentration with time for Concave3 as the mixing time plot is shown in Fig. 16, and the results of its mixing time are shown in Table 7.

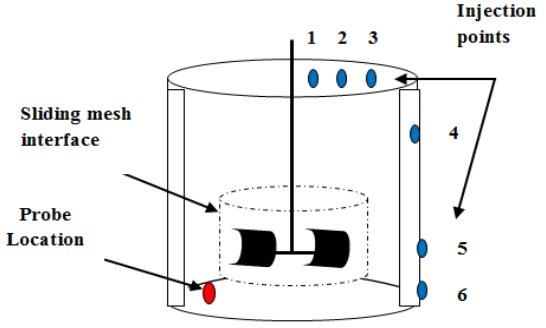

Figure 15. Fluctuations of concentration vs. time for injection in Point 1 and probe.

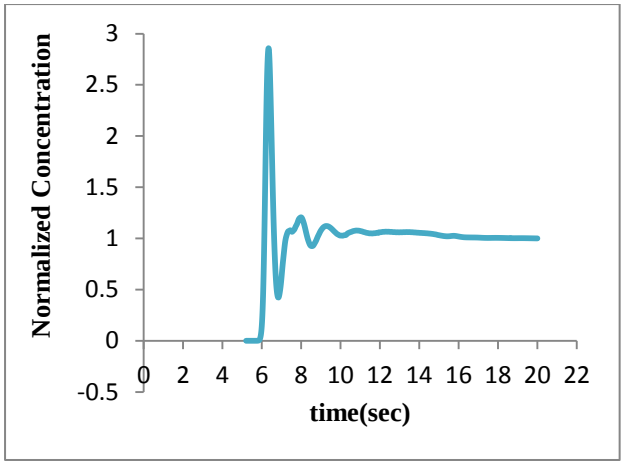

Figure16. Fluctuations of concentration vs. time for injection in Point 1 and probe.

Table 7
Mixing time for different injection points of the optimum impeller.

Injection point	Mixing time ($t_{95\ \%}$, s)	Mixing time($t_{99\ \%}$, s)
1	6.03	9.28
2	6.39	9.84
3	7.93	12.21
4	8.74	13.45
5	7.22	11.11
6	8.18	12.59

Results show that the minimum mixing time occurs for the injection from the top of the vessel on inner rotating cylindrical volume enclosing the impeller and increases by increasing the distance from the impeller to the wall. In the lateral injection, minimum mixing time is in line with the blade. The maximum mixing time for the electrode under the blade is for the lateral injection site (injection point 4), which is located at the top of the disk blade. Injection site 4 is the exchange place of axial flow in the tank.

5. Conclusions

A CFD model was developed to study the baffled stirred vessels with seven types of the concave impeller, and results were compared with a 6-blade Rushton turbine. Investigation of power consumption in different velocities in turbulent flow showed that power was relatively independent of Reynolds number and, for different blades of the concave structure, power consumption was exactly dependent on the shape and geometry of the blades and increased with increasing blade´s angle. The data revealed that the power number was 2.3±0.3 for a blade angle of 40°, whereas, for 25°, 50°, and 55°, it is respectively 43 % lower and 57 % and 43 % higher. This kind of impeller with the vertically asymmetric blade has lower power than Rushton, which has a flat blade. Its shape reduces its power number significantly. Further, changes in power consumption were shown with changes of disc diameter, disc thickness, and different turbulence models. Mixing time was investigated for all impellers with injection above the interface, and results showed Concave6 with much greater height and angle from others has minimum mixing time with maximum power consumption. The optimum impeller was selected on the scale of geometry, power consumption, and mixing time. Changing the probe location at the top and bottom sides of the impeller showed that mixing time was lower for probe under the impeller than that above it. According to the obtained results, all of the concave impellers in this study with asymmetric blades had lower power consumption and almost equal mixing time close to Rushton turbine, and the symmetric concave impeller with lower blade angle had lower power and with major blade angle had major power and lower mixing time than Rushton. The practical and economic benefits of computer simulation have become especially clear when the need for constructing new tanks or components is considered.

Nomenclature

A	area [m^2].
C	concentration of species [kg/m^3].
C_{local}	local instantaneous concentration [kg/m^3].
$\bar{C}_{inst}$	average concentration under instantaneously fully mixed conditions [kg/m^3].
$\hat{C}$	instantaneous normalized local concentration.
D	imeller diameter [m].
D_0	disc diameter [m].
H	tank height [m].
m	number of impeller blades.
N	impeller rotational speed [s^{-1}].
N_p	power number.
Δp	pressure difference [Pa].
p	stirring power input [W].
P	probe.
r	radial direction [m].
R	tank radius [m].
Re	impeller Reynolds number.
t_{inj}	injection time duration [s].
T	tank diameter [m].
u	mean velocity vector [m/s].
V_{tip}	impeller tip velocity [m/s].
w	blade height [m].
X	disc thickness [m].

Greek letters

Z	axial direction [m].
ρ	liquid density [kg/m^3].
Γ	torque [N. m].
μ	liquid viscosity [Pa s].
τ_{ij}	the sub-grid scale stress tensor [Pa].
ν	kinematic viscosity of fluid.

Subscripts

i, j	coordinate directions.

References

[1] Ranade, V. V., Bourne, J. R. and Joshi, J. B., "Fluid mechanics and blending in agitated tanks", *Chem. Eng. Sci.*, **46** (8), 1883 (1991).

[2] Ng, K., Fentiman, N. J., Lee, K. C. and Yianneskis, M., "Assessment of sliding mesh CFD predictions and LDA measurements of the flow in a tank stirred by a Rushton impeller", *Trans. IChemE., Part A*, **76** (6), 737 (1998).

[3] Van't Riet, K. and Smith, J. M., "The behaviours of gas-liquid mixtures near Rushton turbine blades", *Chem. Eng.Sci.*, **28** (4), 1031 (1973).

[4] Van't Riet, K. and Smith, J. M., "The trailing vortex system produced by Rushton turbine agitators", *Chem. Eng.Sci.*, **30** (9), 1093 (1975).

[5] Van't Riet, K., Boom, J .M. and Smith, J. M, "Power consumption, impeller coalescence and rescirculation in aerated vessels", *Trans. IChemE.*, **54** (1), 124 (1976).

[6] Wong, C. W. and Huang, C. T., "Flow characteristics and mechanical efficiency in baffled stirred tanks with turbine impellers", Proceedings of *The 6th European Conference on Mixing*, Pavia, Italy, BHRA, Cranfield, U.K, pp. 29-34 (1988).

[7] Wamoeskerken, M. M. C. G. and Smith, J. M., "The hollow blade agitator for dispersion and mass transfer", *Trans. IChemE., Chem. Eng. Res. Des.*, **67** (2), 193 (1989).

[8] Hjorth, S., US Pat. 4779990, Imeller Apparatus., (1998).

[9] Middleton, J. C, US Pat. 5198156, Agitators., (1993).

[10] Galindo, E. and Nienow, A. W., "Performance of the Scaba 6SRGT agitator in mixing of simulated xanthan gum broths", *Chem. Eng. Technol.*, **16** (2), 102 (1993).

[11] Bakker, A., Myers, K. J. and Smith, J. M., "How to disperse gases in liquids", *Chem. Eng.*, **101** (12), 98 (1994).

[12] Nienow, A. W., "Gas–liquid mixing studies: A comparison of Rushton turbines with some modern impellers",

Chem. Eng. Res. Des., **74** (4), 417 (1996).

[13] Bakker, A., US Pat. 5791780, Impeller Assembly with Asymmetric Concave Blades, (1998).

[14] Pinlli, D., Bakker, A., Myers, K. J., Reeder, M. F., Fasano, J., and Magelli, F., "Some features of a novel gas dispersion impeller in a dual impeller configuration", *Trans. IChemE.*, **81** (4), 728 (2003).

[15] Vlaev, S. D., Staykov, P. and Popov, R., "Pressure distribution at impeller blades of some radial flow impellers in saccharose and xanthan gum solutions a CFD visualization approach", *Trans. IChemE., Part C*, **82** (1), 13 (2004).

[16] Xinhong, L., Yuyun, B., Zhipeng, L. and Zhengming, G., "Analysis of turbulence structure in the stirred tank with a deep hollow blade disc turbine by time-resolved PIV", *Chinese Journal of Chem. Eng.*, **18** (4), 588 (2010).

[17] Jing, Z. H. A. O, Zhengming, G. A. O. and Yuyun, B. A. O., "Effects of the blade shape on the trailing vortices in liquid flow generated by disc turbines", *Chinese Journal of Chem. Eng.*, **19** (2), 232 (2011).

[18] Afshar Ghotli, R., Abdul Aziz, A. R., Ibrahim, Sh., Baroutian,S. and Arami-Niya, A., "Study of various curved-blade impeller geometries on power consumption in stirred vessel using response surface methodology", *Journal of the Taiwan Institute of Chemical Engineers*, **44** (2), 192 (2013).

[19] Ameur, H., "Mixing of shear thinning fluids in cylindrical tanks: Effect of the impeller blade design and operating conditions", *International Journal of Chemical Reactor Engineering*, **14** (5), 1025 (2016).

[20] Wu, H., Patterson, G. K., "Laser-doppler measurements of turblent-flow parameters in a stirrred mixer", *Chemical Engineering Science*, **44** (10), 2207 (1989).

[21] Xuereb, C., and Bertrand, J., "3-D hydrodynamics in a tank stirred by a double-propeller system and filled with a liquid having evolving rheological properties", *Chemical Engineering Science*, **51** (10), 1725 (1996).

[22] Zadghaffari, R., Moghaddas, J. S. and Revstedt, J., "A mixing study in a double-Rushton stirred tank", *Comput. Chem. Eng.*, **33** (7), 1240 (2009a).

[23] Zadghaffari, R., Moghaddas, J. S. and Revstedt, J., "Study of flow field, power and mixing time in a two phase stirred vessel with dual Rushton impellers: experimental observation and CFD simulation", *Chem. Product Process. Model.*, **4** (1), 1 (2009b).

[24] Shekhar, S. M and Jayanti, S., "CFD study of power and mixing time for paddle mixing in unbaffled vessels", *Trans. IChem. E.*, **80** (6), 482 (2002).

[25] Paul, E. L. V. A., Atiemo, O. and Kresta, S. M., Handbook of indstrial mixing: science and practice, 3rd ed., New Jersey, John Wiley & Sons, p.145 (2004).

[26] Brucato, A., Ciofalo, M., Grisafi, F. and Micale, G., "Numerical prediction of flows in baffled stirred vessels: A comparison of alternative modelling approaches", *Chemical Engineering Science*, **53** (21), 3653 (1998).

[27] Myers, K. J., Thomas, A. J., Bakker, A. and Reeder, M. F., "Performance of a gas dispersion impeller with vertically asymmetric blades", *Trans IChemE.*, **77** (8), 728 (1999).

[28] Yapici, K., Karasozen, B., Schafer, M. and Uludag,Y., "Numerical investigation of the effect of the Rushton type turbine design factors on agitated tank flow characteristics", *Chemical Engineering and Processing*, **47** (8), 1340 (2008).

[29] Zadghaffari, R., Moghaddas, J. S. and Revstedt, J., "Large-eddy simulation of turbulent flow in a stirred tank driven by a Rushton turbine", *Comput. & Fluid*, **39** (7), 1183 (2010).